Published in final edited form as:
Dev Cell. 2017 March 13; 40(5): 505–511.e6. doi:10.1016/j.devcel.2017.02.009.

Cell-cell contact area affects Notch signaling and Notch-dependent patterning

Oren Shaya[1,9], **Udi Binshtok**[1,9], **Micha Hersch**[2,3], **Dmitri Rivkin**[1], **Sheila Weinreb**[1], **Liat Amir-Zilberstein**[1], **Bassma Khamaisi**[1], **Olya Oppenheim**[1], **Ravi A. Desai**[4,5], **Richard J. Goodyear**[6], **Guy P. Richardson**[6], **Christopher S. Chen**[7,8], and **David Sprinzak**[1,10,*]

[1]Department of Biochemistry and Molecular Biology, Wise Faculty of Life Science, Tel Aviv University, Tel Aviv 69978, Israel [2]Department of Medical Genetics, University of Lausanne, Lausanne CH-1015, Switzerland [3]Swiss Institute of Bioinformatics, Lausanne CH-1015, Switzerland [4]University College London, Department of Cell and Developmental Biology and Institute for Physics of Living Systems, London WC1E 6BT, UK [5]The Francis Crick Institute, London NW1 1AT, UK [6]Sussex Neuroscience, School of Life Sciences, University of Sussex, Falmer, Brighton BN1 9QG, UK [7]The Biological Design Center and Biomedical Engineering, Boston University, Boston, MA 02215, USA [8]The Wyss Institute for Biologically Inspired Engineering, Harvard University, Boston, MA 02115, USA

Summary

During development, cells undergo dramatic changes in their morphology. By affecting contact geometry, these morphological changes could influence cellular communication. However, it has remained unclear whether and how signaling depends on contact geometry. This question is particularly relevant for Notch signaling, which coordinates neighboring cell fates through direct cell-cell signaling. Using micropatterning with a receptor trans-endocytosis assay, we show that signaling between pairs of cells correlates with their contact area. This relationship extends across contact diameters ranging from microns to tens of microns. Mathematical modeling predicts that dependence of signaling on contact area can bias cellular differentiation in Notch-mediated lateral inhibition processes, such that smaller cells are more likely to differentiate into signal-producing cells. Consistent with this prediction, analysis of developing chick inner ear revealed that ligand-producing hair cell precursors have smaller apical footprints than non-hair cells. Together, these results highlight the influence of cell morphology on fate determination processes.

*Correspondence: Further information and requests for resources and reagents should be directed to and will be fulfilled by the Lead Contact ,David Sprinzak (davidsp@post.tau.ac.il).
[9]Co-first author
[10]Lead Contact

Author Contribution

Conceptualization, O.S., U.B., and D.S.; Methodology, R.A.D. and C.S.C.; Software, U.B., M.H., and D.R.; Investigation, O.S., U.B., M.H., D.R., S.W., L.A.Z., B.K., and O.O.; Writing – Original Draft, O.S., U.B., and D.S.; Writing – Review & Editing, O.S., U.B., M.H., R.G., G.R, C.S.C, R.A.D, and D.S.; Funding Acquisition, D.S.; Resources, R.G. and G.R.; Supervision, D.S.

Data and Software Availability

All simulations and analysis was performed using custom code written in Matlab (the MathWorks Inc.). All simulation code used in this study is available for download in https://github.com/Udi-Binshtok/Dimensionless-equations-simulator_-February-2017.git

Europe PMC Funders Author Manuscripts

Keywords

Notch signaling; lateral inhibition; cell morphology; live cell imaging; cell-cell contact; inner ear

Europe PMC Funders Author Manuscripts

Introduction

Many developmental processes involve changes in cell morphology that occur concurrently with cell fate decision processes. Examples include epithelial to mesenchymal transitions (Thiery, 2003), switching between tip and stalk cell fates during angiogenesis (Jakobsson et al., 2010), and cell fate decisions controlled by the formation of filopodia (Cohen et al., 2010; Kornberg and Roy, 2014). Despite these observations, the morphological aspects of differentiation are often treated as a downstream consequence of fate-specific gene expression and are not considered as an essential part of the cell fate decision process. One way in which changes in cell morphology can affect cell fate decision processes is by affecting the magnitude of signaling between cells. This concept has been discussed in various contexts including for example in angiogenesis (Bentley et al., 2009; Bentley et al., 2014), bristle patterning in *Drosophila* (Hunter et al., 2016), and asymmetric cell divisions in zebrafish (Akanuma et al., 2016). Nevertheless, we still lack direct evidence for the dependence of signaling on cell morphology and how it affects cell fate decision processes.

Here we study the effect of cell morphology on the highly conserved Notch signaling pathway, which is ubiquitously used for coordination of differentiation between neighboring cells in processes such as boundary formation and lateral inhibition (Artavanis-Tsakonas and Muskavitch, 2010; Artavanis-Tsakonas et al., 1999). Notch signaling relies on the interaction between Notch receptors and the Delta-Serrate-Lag2 (DSL) ligands at the boundary between neighboring cells (Bray, 2006; D'Souza et al., 2010). It is known to mediate cell-cell communication through a variety of contact morphologies, ranging from relatively broad adherens junctions (Benhra et al., 2010; Couturier et al., 2012) to submicron filopodial contacts (Cohen et al., 2010; Hamada et al., 2014; Huang and Kornberg, 2015). The large variance in contact sizes raises the question of how Notch signaling depends on contact area. Based on the analysis of diffusion and endocytosis rates of Notch ligands, we recently predicted that there could be two distinct behaviors for the contact area dependence (Khait et al., 2015). Notch signaling could be either proportional to the contact area if diffusion is relatively slow, or could be independent on contact area, for relatively fast diffusion. Here, we wanted to directly test the dependence of Notch signaling on contact area and to understand whether such dependence could affect Notch-mediated patterning.

Results

To understand the dependence of Notch signaling on the dimensions of the contact area between cells, we wanted to develop a method that allows a direct measure of the interactions between Notch receptors and ligands in a controlled cellular geometry. To achieve that, we combined micropatterning technology with a live-cell trans-endocytosis (TEC) assay to track the dynamics of Notch1 (N1) and Delta-like 1 (Dll1) interactions between pairs of cells in a controlled geometry. The Notch TEC assay is based on measuring

the amount of Notch extra cellular domain (NECD) that trans-endocytoses into the ligand-expressing cell following its interaction with the DSL ligand (Heuss et al., 2008; Nichols et al., 2007; Parks et al., 2000). In this assay, we used fusion constructs in which both the extracellular domain of Notch 1 and the C-terminus of the ligand Delta-like-1 are labeled with fluorescent protein tags (Fig. 1A). To label N1, we introduced citrine between the EGF-like repeats and the negative regulatory region in the extracellular domain (between G1435 and A1436) (Fleming et al., 2013). In most of our experiments, we used a variant of human N1 in which the intracellular domain was replaced with a transcriptional activator Gal4 to avoid activation of endogenous Notch targets (Sprinzak et al., 2010). The resulting fusion construct (N1G4-citrine) exhibited similar activity in a reporter assay as the N1G4 construct without the citrine tag (Fig. S1A). For tracking Dll1 dynamics, we used a c-terminal fusion of rat Dll1 and mCherry under a doxycycline inducible promoter (Sprinzak et al., 2010). We generated stable cell lines in Chinese Hamster Ovary cells (CHO-K1) which express either the N1G4-citrine or the Dll1-mCherry.

To observe TEC dynamics, N1G4-citrine and Dll1-mCherry cells were co-cultured and imaged using live-cell confocal microscopy (Fig 1B,C). We induced the expression of Dll1-mCherry and tracked the fluorescence of both N1G4-citrine and Dll1-mCherry in regions where the two cell types come in contact. About two hours after Dll1-mCherry induction, we observed TEC of N1G4-citrine into the Dll1-mCherry cells, mostly in the form of vesicles containing both N1G4-citrine and Dll1-mCherry (Fig. 1C, movie S1). No TEC is observed where Dll1-mCherry cells are not in contact with N1G4-citrine cells or when Dll1-mCherry is not induced (Fig. S1B-G). TEC is also observed in similar assays in which full-length N1 expressing cells are co-cultured with Dll1-mCherry cells (Fig. S1H-J) or when Dll1-mCherry is expressed in Marin Darby Canine Kidney (MDCK) cells instead of CHO-K1 cells (Fig. S1K-M). These show that TEC is a general feature of N1-Dll1 interactions and is not specific to the Notch variant or the cell line used.

To understand the relation between TEC in the sending cells and the transcriptional response in the receiving cells, we generated a stable cell line having both N1G4-Citrine and a transcriptional reporter activated by Gal4 (UAS-H2B-mCherry)(Sprinzak et al., 2010). Co-culture experiments between these reporter cells and Dll1-mCherry cells show that the level of the transcriptional reporter is correlated with the level of TEC in the adjacent sending cell, albeit with a mean delay of 255±29 minutes (obtained from 6 movies such as the one shown in Fig. S1N-P). This delay reflects the relatively slow response of the transcriptional reporter in the receiving cell. The TEC signal on the other hand, is observed without any delay. Furthermore, we noticed that the TEC decayed with a half-life of about 60 minutes in a movie in which the receiver and sender cells detach (Fig. S1Q-R). Hence, the TEC provides a direct measure of signaling dynamics between cells.

To study the dependence of Notch signaling on contact area we used a micro-patterned device termed 'the two-cell assay', which restricts pairs of cells to predefined bowtie shaped microwells on a glass bottom dish (Desai et al., 2009) (Fig. 2A). The microwells were typically 20μm in diameter and were connected by a 2-5μm wide neck. By randomly seeding N1G4-citrine and Dll1-mCherry cells, we got many microwells with mixed pairs (i.e. one cell from each type in the same bowtie device). Time-lapse movies of N1G4-citrine and

Dll1-mCherry cell pairs were acquired upon induction of Dll1-mCherry by doxycycline (Fig. 2B-G). The TEC signal was defined as the citrine fluorescence measured within the boundaries of the Dll1-mCherry cell. We typically observe that the TEC levels increase with the levels of Dll1-mCherry in the first few hours of the movie (Fig. 2D,G,H,I, movies S2, S3). Unexpectedly, the TEC saturates or even decreases at longer times, even though ligand levels continue to increase (Fig. 2D,G,H,I, movies S2, S3). This unexpected pulse-like behavior in TEC is observed in the majority of cell pairs recorded (Fig. S2A) and is qualitatively similar to the behavior observed in free co-culture (not shown).

To test the effect of contact area on TEC, we performed the two-cell TEC assay on cell pairs with varying contact widths. Although the two-cell assay generally restricts the cells to the bowtie shaped microwells, the actual contact area between cells varied considerably between pairs. Furthermore, we had instances in which cells partially break out of the microwells generating situations with relatively large contact areas (Fig. 2E-G, movie S3). We typically observe more TEC vesicles in cell pairs with larger contacts.

To quantitatively compare TEC from different pairs of cells, we needed to take into account the dependence of TEC on the expression level of Dll1-mCherry, which varies between cell pairs. Since during the initial increase phase, the TEC is generally proportional to the Dll1-mCherry level (Fig. S2E), we looked at the TEC levels normalized by Dll1-mCherry levels in each pair (denoted as normalized TEC (nTEC)). A comparison of the nTEC between the two pairs in Figs. 2B-D,H and 2E-G,I showed that nTEC for the pair with larger contact width is up to 5 times higher than the nTEC for the pair with the small contact width (Fig. 2J).

We note that in some cases we observe cell divisions either before or during the measurements (see grayed area in Fig. 2I, and dashed lines in Fig. S2A). We analyzed all cases where cell divisions occurred in the sender cells and identified two scenarios: (1) The Dll1 cell divides, and both daughter cells remain in contact with the receiver (parallel signaling). (2) The Dll1 cell divides but only one cell stays in contact (single cell contact). To take into account sender cell division in our analysis, we calculate nTEC only in the sender cell (or cells) that come in contact with the receiver cell. Some of the N1G4-Citrine cells also divide, but in general, this does not seem to affect nTEC levels (no significant change after cell division).

To check the relation between contact width and TEC, we repeated the analysis shown in Fig. 2J in multiple cell pairs. We compared the nTEC levels between cell pairs at the first few hours after induction. We chose to look at nTEC between 90-150 min where significant TEC is already observed in most cell pairs and still correlates with Dll1-mCherry levels (i.e. before the peak in TEC). We note that the widths of the contact areas do not change significantly during the 0-150 minute time frame (Fig. S2B), nor do they vary significantly along the z-direction over most of the cell height (Fig. S2C-D). We find that nTEC significantly correlates with contact width over a range of contact widths from ~1-40 μm (Fig. 3, $\rho=0.83$, p-value$<10^{-8}$). The peak values of nTEC (termed max nTEC) also show significant correlation with contact widths (Fig. S3, $\rho=0.72$, p-value$<10^{-5}$). We note that repeating this analysis on one pair of cells identified in standard co-culture conditions (Such

as the ones in Fig. 1C) gave results that are consistent with the general trend observed in Fig. 2J (see point marked by square in Fig. 3 and Fig. S3). The observed correlation of nTEC with contact width strongly supports a model in which larger contact area results in more N1-Dll1 pairs interacting with each other and to more signaling.

We next wanted to understand the implications of the observed contact area dependence of Notch signaling on Notch dependent patterning. In particular, we focus on lateral inhibition patterning, which is often employed to generate checkerboard-like patterning in multiple developmental contexts (Artavanis-Tsakonas et al., 1999). Models of lateral inhibition rely on an intercellular feedback circuit that amplifies small initial differences in the levels of Notch signaling between neighboring cells (Fig. 4A) (Collier et al., 1996; Formosa-Jordan and Sprinzak, 2014; Shaya and Sprinzak, 2011; Sprinzak et al., 2011). This feedback leads to a checkerboard-like pattern where some cells are selected to become sender cells (‘high Delta cells’), each of which is surrounded by receiver cells (‘low Delta cells’) (Fig. 4B).

To check the effect of cell morphology on lateral inhibition patterning, we developed a lateral inhibition model that takes into account the dependence of Notch signaling on contact area (Fig. 4A, methods). In our model, we explicitly calculate the concentrations of Notch and Delta on each boundary of each cell. The dependence on the contact area is taken into account by integrating the signal resulting from Notch-Delta interactions over the length of each boundary. We ran the model simulations on disordered cell lattices that contained cells with different sizes (Fig. 4B). For simplicity, we assumed that cell lattices are fixed (equivalent to assuming that fate determination is faster than changes in cell morphology).

Our simulations reveal that the linear dependence of signaling on contact area leads to a significant bias in the selection of fates in such a model; the smallest cells typically tend to become high Delta cells, while the largest cells typically tend to become low Delta cells. To check the significance of this effect we ran simulations on 20 randomly generated lattices and plotted the distribution of perimeters for high- and low-Delta cells (Fig. 4C). Indeed, the distribution of high Delta cells (red bars in Fig. 4C) is significantly shifted with respect to the low-Delta cells (green bars in Fig. 4C). To verify that the effect is due to dependence on contact area and not on the number of neighbors, we also performed the simulations on random cell lattices that retain hexagonal geometry (e.g. each cell has exactly 6 neighbors) but still have different cell sizes. The results of these simulations also exhibit a significant bias of high Delta cells to smaller perimeters (Fig. S4A-B). We note that running the simulation on a hexagonal lattice without taking into account the contact area dependence results in random selection of high Delta cells as reported previously (Collier et al., 1996; Sprinzak et al., 2011).

To understand where the bias on cell size comes from, we checked how the level of inhibitory signals in the cells behaves at early time points when fate is being determined. We define the 'fate determination time' as the latest time point where the Delta levels of the prospective high and low Delta cells cannot be statistically distinguished (inset of Fig. 4D). We find that at the fate determination time, the level of inhibitory signal, represented by the level of an intracellular repressor of Delta, R, which is directly activated by Notch signaling

(Fig. 4A and methods), is correlated with cell perimeter (Fig. 4D). This shows that the bias in cell fate arises from an early bias in Notch signaling due to differences in cell perimeters.

To test the prediction of our model, that smaller cells are more likely to become high-Delta cells, we looked at the classical Notch-mediated lateral inhibition process in the chick basilar papilla (Goodyear and Richardson, 1997). In this system, an initially undifferentiated field of cells differentiates into an alternating pattern of hair cells and supporting cells. We have analyzed images from chick basilar papilla at embryonic days 6 to 8 (E6 – E8) stained with a membrane marker and hair cell antigen marker (HCA). At this developmental stage, the first presumptive hair cells (HCA-positive cells) appear, first in the distal (E6) and later at the medial and proximal (E7-E8) regions of the basilar papilla (Goodyear and Richardson, 1997). Our analysis reveals that at this early onset stage of hair cell selection we indeed see that HCA-positive cells are predominantly selected from cells with smaller apical perimeters (Fig. 4E-F and Fig. S4C-I). We note that Notch-Delta interactions in epithelial layers are typically restricted to adherens junctions at the apical surface (Benhra et al., 2010; Hatakeyama et al., 2014) justifying the quasi-two dimensional analysis performed here. We also note that HCA-positive cells tend to become larger (rather than smaller) at later developmental stages (Goodyear and Richardson, 1997), suggesting that hair cell selection does not lead to a smaller cell phenotype. Hence, this observation is consistent with the prediction of our model that cell size can bias cell fate decision processes.

Discussion

Our two-cell TEC assay experiments provide the first direct evidence that Notch signaling depends on the contact area between cells. We have recently shown in a theoretical model (Khait et al., 2015) that Notch signaling may not necessarily depend on contact area. For example, if the receptors and ligands can diffuse quickly on the cell membrane or if the contact area is small enough, a significant contribution to the resulting signal may come from receptors and ligands that diffuse into the contact area from nearby membrane regions. In this case, we would expect the signal to depend very weakly on the contact area. The theoretical analysis showed that depending on the ratio between the contact diameter and the diffusion length scale (i.e. the typical distance ligands and receptors diffuse on the cell membrane before they endocytose), signaling could either depend on contact area or be independent of contact area. Hence, the observation here that Notch signaling depends on contact area is an indication we are in the 'slow diffusion regime' where the contact area is larger than the diffusion length scale. This is consistent with our previous measurements showing that the diffusion length scale of Dll1 is about 1-2μm. Hence, our results show that at least for typical epithelial cell-cell contact diameters, it is expected that signaling should depend on contact area.

We note, that in our lateral inhibition model (Fig. 4) we did not take into account the effect of membrane diffusion of Notch receptors and ligands, nor the situation of signaling through filopodia with very small contact diameters. It will be interesting to understand the role of diffusion and signaling through filopodia on cell fate determination, by considering expanded models that take these into account.

Our measurements also revealed an unexpected decrease or saturation in the TEC signal after a few hours, even though the level of ligand continues increasing (Fig. 2H-I). This pulse-like response suggests that there may be some limiting factor that prevents further signaling at a certain time point or signaling level. We note that at longer times we still observe both N1G4-citrine and Dll1-mCherry at the cell surface (not shown), ruling out the possibility that surface levels of either the ligands or the receptors are these limiting factors. Hence, the mechanism for this unexpected dynamic behavior still needs to be elucidated.

The observed dependence of Notch signaling on contact diameter can have implications on Notch dependent patterning processes such as lateral inhibition (Heitzler and Simpson, 1991). We show that a model of lateral inhibition that takes into account contact area dependence predicts that smaller cells are more likely to be selected by the lateral inhibition process than larger cells. Such behavior is indeed observed during the early development of chick inner ear. More generally, this result strongly suggests that cell fate decision processes are controlled not only by biochemical regulatory processes, but can also be affected by changes in cellular morphology. Hence, a systems level approach that takes into account both regulatory circuits and cellular morphology is required for understanding such developmental patterning processes. This result should be relevant for other juxtacrine signaling pathways as well as for other developmental processes controlled by juxtacrine signaling pathways.

Star Methods

Experimental Model and Subject Details

Base Cell lines—Chinese Hampster ovary cells (CHO-K1, ATCC-CCL-61) integrated with TetR (Life Technologies, CHO-TR). Organism: Cricetulus griseus. Sex: female.

Marine Darby Canine Kidney (MDCKII, ATCC-CRL-2936). Organism: Canis familiaris. Sex: female.

Chick Basilar Papilla—All chick Basilar Papilla images are based on analysis of partially published images taken from (Goodyear and Richardson, 1997). The description of sample preparation is described in (Goodyear and Richardson, 1997). In brief, chicken eggs of the Isa Brown variety were incubated at 37°C in a humid incubator for between 6 and 8 days. Whole heads from embryos of embryonic day (E) 6 and 8 were fixed in 3.7% (v/v) formaldehyde in 100 mM sodium phosphate buffer, pH 7.2, for 1 hr at room temperature.

Method Details

Description of genetic constructs—All genetic constructs were constructed using standard cloning techniques. The Dll1-mCherry, hN1, and the N1G4 constructs were described previously (Sprinzak et al., 2010). The UAS-H2B-mCherry was cloned from the UAS-H2B-citrine construct used in (Sprinzak et al., 2010). The N1G4-citrine construct was constructed using Gibson cloning (Gibson et al., 2009). The N1G4-citrine was constructed from pcDNA3-hNECD-Gal4esn described in previous work (Sprinzak et al., 2010). It contains the extracellular domain (ECD) of human Notch1 whereas the intracellular domain is replaced with a minimal variant of the transcriptional activator Gal4, termed as Gal4esn.

In this work, the citrine gene, flanked by GSG linkers on both sides, was inserted into the extracellular domain of human Notch1, between G1435 and A1436.

The position has been successfully used in Drosophila Notch for EGFP tagging (Fleming et al., 2013). Three overlapping fragments of the vector and one insert fragment were amplified using PCR (Platinum pfx, Life Technologies). The primers used for the amplification of the citrine insert are provided in the KRT table. The primers used for the amplification of the three overlapping fragments of the pcDNA3-hNECD-Gal4esn are also provided in the KRT table. All four fragments were then assembled into the final construct using the Gibson protocol (Gibson et al., 2009).

Generation of stable cell lines and cell-culture protocols—The CHO-Dll1-mCherry was described previously (Sprinzak et al., 2010). The MDCK-Dll1-mCherry cell line was generated using the same procedures as the CHO-Dll1-mCherry but with MDCKII as a base cell line (ATCC CRL-2936), In brief, cells were transfected with Dll1-mCherry construct, after two days transferred to a 6 well plate and placed under selection for 100ng/ul Hygromycin for two weeks. Single colonies are then isolated using limiting dilution. The CHO-N1G4-citrine was also generated by transfecting CHO-TR cells (Life Technologies) with the N1G4-citrine construct following selection with 10μg/ml Blasticidine (Scientific inc.) and 625 μg/ml Geneticin (Life Technologies). Colonies were picked up and tested for fluorescence and activity. The CHO-N1G4-citrine+UAS-H2B-mCherry reporter cells were generated by stable transfection of the UAS-H2B-mCherry reporter in to the CHO-N1G4-citrine cells and selection of single clones using 400ug/ml Zeocin (Invivogen inc.).

Notch Activity assay—The activity of N1G4-citrine was tested using luciferase reporter gene assay. N1G4-citrine cells and N1G4esn cells (Sprinzak et al., 2010) were co-transfected in 24-well dishes using TransIT-LT1 (Mirus) with a Gal4-firefly luciferase reporter (Andrawes et al., 2013) (800 ng) and pRL-SV40 Renilla luciferase (10 ng). 24 hours after transfection, the cells were trypsinized and transferred to dishes with or without plate-adsorbed Delta-like 1 fused to immunoglobin-G (Dll1-Fc, a kind gift from Irwin Bernstein). Coating of adsorbed Dll1-Fc was performed by incubating 5ng/μl of Dll1-Fc for 1h at 4C. 48 hours after plating, firefly luciferase and Renilla luciferase activities were measured by luminumeter (Veritas). Cells were lysed with 100 μl/well Passive lysis buffer x1 (promega) for 10 min. 20μl of each sample was used for luciferase activity using filtrated luciferase buffer including: 26 mg of (MgCO3)4 Mg(OH)2 (Sigma), 20 mM Tricine (Sigma), 0.1 mM EDTA (Biological Industries), 2.67 mM pH=7.8 MgSO4 (Merck). For the luciferase reaction we used luciferase buffer supplemented with: 0.4 mM ATP (Sigma), 26.6 mM DTT (Sigma), Coenzyme A X0.8 (Sigma) AND 0.4 mM D-Luciferine and for Renilla activity using filtrated Renilla buffer including 80 mM di-Potassium hydrogen phosphate trihydrate (Merck) and 20 mM Potassium dihydrogen phosphate for analysis (Merck). Notch activity is expressed as a ratio of normalized luciferase between cells exposed to dishes with and without plated Dll1-Fc. The assay was repeated five times.

Micropatterning—Micropatterning was performed as previously described (Desai et al., 2009). In brief, A PDMS mold with raised bowtie patterns was attached to a glass surface after being treated with a UV/Ozone cleaning device (UVOCS, USA). Liquid agarose (0.6%

in 2:3 EtOH:diH_2O) was wicked into the gap between the mold and the glass and an inverted pattern of agarose was formed upon removal of the PDMS mold. Bovine Fibronectin (50 μg/ml, Biological Industries, Israel) was adsorbed on the exposed regions of the glass by incubating it for 1hr at room temperature. Both N1G4-citrine and Dll1-mCherry cells were diluted to 1.25×10^5 cell/ml and seeded simultaneously onto the patterned plate. The square size of the bowties used was 20x20μm which yielded the highest probability of a single cell to attach in each half of the bowtie.

Preparation of cells for imaging—For the two-cell assay, cells were seeded 12 hours before imaging in growth medium (αMEM+10% fetal bovine serum, Biological Industries, Israel) onto agarose micropatterns constructed on home-made glass bottom 6-well plates. Directly prior imaging the media was replaced with low fluorescence imaging media (αMEM without Phenol red, ribonucleosides, deoxyribonucleosides, folic acid, biotin and vitamin B12, Biological Industries, Israel) and 100ng/ml doxycycline (Sigma-Aldrich) was added to the growth medium to induce expression.

Immunohistochemistry—Immunohistochemisty was performed in order to establish the TEC of full length Notch1 and Dll1-mCherry (Fig. S1H-J). CHO-K1 cells expressing full length Notch1(Sprinzak et al., 2010) were co-cultured with Dll1-mCherry cells for 24 hours prior to fixation and staining. 100 ng/ml doxycycline was added to the co-culture 5 hours prior to fixation and staining. The cells were fixed with 4% paraformaldehyde (Merck), permeabilized using triton (Sigma Aldrich) and immunostained with anti-mouse-Notch1 (1:100) antibody (R&D systems) for 1 hour at room temperature. After incubation the cells were washed three times with phosphate buffer saline (Biological Industries). Secondary antibody, Alexa Flour 488-conjugated AffiniPure Rabbit-anti-Sheep (1:200, Jackson ImmunoResearch), was added for 45 minutes at room temperature. Cells were washed again as described.

Microscopy details—Cells were imaged using Andor revolution spinning disk confocal microscope with DPSS CW 515nm and 561nm 50mW lasers (Andor, Belfast, Northern Ireland). The imaging setup consisted of an Olympus inverted microscope with an oil-immersion Plan-Apochromatic 60x objective NA=1.42 (Olympus, Tokyo, Japan); and an ANDOR iXon Ultra EMCCD camera (Andor, Belfast, Northern Ireland). The microscope was equipped with a 37 °C temperature-controlled chamber and a CO_2 regulator providing 5% CO_2 (Okolab, Italy). The equipment was controlled by Andor iQ software (Andor, Belfast, Northern Ireland).

Chick Basilar Papilla staining—The description of sample preparation is described in (Goodyear and Richardson, 1997). In brief, chick basilar papilla at embryonic day 6 (E6) and embryonic day 8 (E8) were stained using both anti-cingulin (membrane marker) and anti-HCA (Hair cell marker).

Mathematical model—To model the effect of the contact-dependent Notch signaling on lateral inhibition patterning, we expanded a model previously described in (Sprinzak et al., 2010) to take into account contact area dependence. For simplicity, cis-interactions between receptors and ligands (Sprinzak et al., 2010) are not considered in this model. We verified

that inclusion of cis-inhibition does not change the conclusions provided here (not shown). We simulated Notch mediated lateral inhibition circuit on a disordered two-dimensional lattice (as shown in Fig. 4A-B). Cells on the lattice have different fixed contact areas and hence our model takes into account that Notch signaling should vary between cells and between boundaries. We note that cells' size and boundaries are constant in time. To describe the amount of signal between neighboring cells, we look on the concentration of Notch and Delta on both sides of the boundary. We denote n_{ij} as the concentration of Notch in cell i on the boundary with cell j. Similarly, d_{ji}, is the concentration Delta in cell j on the boundary with cell i.

The signal concentration (number of NICD produced per unit length) generated into the i-th cell at boundary ij, denoted s_{ij}, is described by Michaelis-Menten reaction:

$$n_{ij}+d_{ji} \underset{\kappa^-}{\overset{\kappa^+}{\rightleftharpoons}} [n_{ij}d_{ji}] \xrightarrow{\kappa^s} s_{ij} \quad (1)$$

Where $[n_{ij}d_{ij}]$ denotes the concentration of complexes of Notch and Delta on the boundary between cell i and cell j (in this case the complexes composed of Delta from cell j bound to Notch from cell i). κ^+, κ^- are the association and dissociation rates of Notch and Delta, respectively. κ^S, is the rate associated with conversion of the Notch-Delta complex into a signal (namely, the inverse time it takes for the NICD to get cleaved once it interacts with Delta)

According to Fig. 3, we assume a linear relation between the total signal and the contact area. That is, the total signal received by cell i is the summation of all signal concentration on all of its boundaries times the length of each boundary:

$$S_i = \sum\nolimits_j s_{ij} l_{ij} \quad (2)$$

The lateral inhibition feedback is considered by assuming that a repressor with total cellular expression level, R_i, is activated by the total signal in each cell, S_i, and that this repressor inhibits the production of total Delta in cell i,

$$S_i \rightarrow R_i \dashv D_i \quad (3)$$

The activation and repression reactions in eq. 3 are described in terms of Hill functions. These reactions can be written in terms of a set of ordinary differential equations for each boundary in the system:

$$\frac{dn_{ij}}{dt} = \frac{\beta_N}{L_i} - \gamma_N n_{ij} + \kappa^- [n_{ij}d_{ji}] - \kappa^+ n_{ij} d_{ji} \quad (4)$$

$$\frac{dd_{ij}}{dt}=\frac{\beta_D}{L_i}\frac{p_R^l}{p_R^l+R_i^l}-\gamma_D d_{ij}+\kappa^-\left[n_{ji}d_{ij}\right]-\kappa^+ n_{ji}d_{ij} \quad (5)$$

$$\frac{dR_i}{dt}=\beta_R\frac{S_i^m}{p_S^m+S_i^m}-\gamma_R R_i \quad (6)$$

$$\frac{d\left[n_{ij}d_{ji}\right]}{dt}=\kappa^+ n_{ij}d_{ji}-\kappa^-\left[n_{ij}d_{ji}\right]-\kappa^s\left[n_{ij}d_{ji}\right] \quad (7)$$

$$\frac{ds_{ij}}{dt}=\kappa^s\left[n_{ij}d_{ji}\right]-\gamma_S s_{ij} \quad (8)$$

Here, L_i is the perimeter of cell i. β_N, β_D and β_R are the production rates of total Notch, Delta and Repressor, respectively. γ_N, γ_D, γ_R, and γ_S are the degradation rates of Notch, Delta, Repressor, and Signal, respectively. p_R, l, p_S and m describe the effective K_d and Hill coefficients of the Repressor and the total Signal, respectively. The number of equations for Notch, Dalta, Notch-Delta complex, and Signal is twice the number of boundaries in the system. The number of equations for the Repressor is equal to the number of cells.

We assume here that Notch and Delta distribute uniformly across the perimeter of the cell after being produced. As in (Sprinzak et al., 2010), we also assume that the complexes and the signal reach stable state much faster than Notch, Delta and the Repressor. In that case equations 7 and 8 become:

$$\frac{d\left[n_{ij}d_{ji}\right]}{dt}\simeq 0\Rightarrow\left[n_{ij}d_{ji}\right]\simeq\frac{\kappa^+}{\kappa^-+\kappa^s}n_{ij}d_{ji} \quad (9)$$

$$\frac{ds_{ij}}{dt}\simeq 0\Rightarrow s_{ij}\simeq\frac{\kappa^s}{\gamma_S}\left[n_{ij}d_{ji}\right]\simeq\frac{\kappa^s}{\gamma_S}\frac{\kappa^+}{\kappa^-+\kappa^s}n_{ij}d_{ji} \quad (10)$$

This leads to the final set of equations:

$$\frac{dn_{ij}}{dt}=\frac{\beta_N}{L_i}-\gamma_N n_{ij}-\frac{\kappa^+\kappa^s}{\kappa^-+\kappa^s}n_{ij}d_{ji} \quad (11)$$

$$\frac{dd_{ij}}{dt}=\frac{\beta_D}{L_i}-\frac{p_R^l}{p_R^l+R_i^l}-\gamma_D d_{ij}-\frac{\kappa^+\kappa^s}{\kappa^-+\kappa^s}n_{ji}d_{ij} \quad (12)$$

$$\frac{dR_i}{dt}=\beta_R\frac{\left(\sum_j\frac{1\kappa^+\kappa^s}{\gamma_S\kappa^-+\kappa^s}n_{ij}d_{ji}l_{ij}\right)^m}{p_S^m+\left(\sum_j\frac{1\kappa^+\kappa^s}{\gamma_S\kappa^-+\kappa^s}n_{ij}d_{ji}l_{ij}\right)^m}-\gamma_R R_i \quad (13)$$

The total free Notch and free Delta proteins in cell *i* are the summation of all protein concentration on all of its boundaries times the length of each boundary:

$$N_i=\sum_j n_{ij}l_{ij};\ D_i=\sum_j d_{ij}l_{ij} \quad (14)$$

To simplify the model we transformed the variables and parameters of equations 11-13 to dimensionless variables and parameters:

$$t\to\gamma_R t\ ;\ \tau_N\equiv\frac{\gamma_R}{\gamma_N}\ ;\ \tau_D\equiv\frac{\gamma_R}{\gamma_D}\ ;\ \beta_N\to\frac{\beta_N}{\gamma_N n_o\hat{L}}\ ;\ \beta_D\to\frac{\beta_D}{\gamma_D d_o\hat{L}}\ ;\ \beta_R\to\frac{\beta_R}{p_{R\gamma R}}$$

$$R\to\frac{R}{p_R}\ ;\ n\to\frac{n}{n_0}\ ;\ d\to\frac{d}{d_0}\ ;\ L\to\frac{L}{\hat{L}}\ ;\ l\to\frac{l}{\hat{L}}\ ;\ \kappa_t^{-1}\equiv\frac{d_o}{\gamma_N}\frac{\kappa^+\kappa^s}{\kappa^-+\kappa^s}$$

Where $\hat{L}$ is the average cell perimeter (averaged over all the cells in the simulated lattice).

We also assumed the following constraints:

$$\gamma_N=\gamma_D=\gamma_R\ ;\ \frac{d_o}{\gamma_N}=\frac{n_o}{\gamma_D}\ ;\ p_S\frac{\gamma_S(\kappa^-+\kappa^s)}{n_0 d_0\hat{L}\kappa^+\kappa^s}=1$$

That leads to the following dimensionless model:

$$\frac{dn_{ij}}{dt}=\frac{\beta_N}{L_i}-n_{ij}-\kappa_t^{-1}n_{ij}d_{ji} \quad (15)$$

$$\frac{dd_{ij}}{dt}=\frac{\beta_D}{L_i}\frac{1}{1+R_i^l}-d_{ij}-\kappa_t^{-1}n_{ji}d_{ij} \quad (16)$$

$$\frac{dR_i}{dt}=\beta_R\frac{(\Sigma_j n_{ij}d_{ji}l_{ij})^m}{1+(\Sigma_j n_{ij}d_{ji}l_{ij})^m}-R_i \quad (17)$$

These equations (15-17) are solved numerically using ordinary differential equation solver (ODE) in Matlab on 20 different random lattices.

Generation of random lattices—The cell lattices were generated by starting from an initial 12 by 12 regular hexagonal lattice with periodic boundary conditions, i.e., disposed on a torus topology with up joining down and left joining right. The lattices were implemented as vertex models similar to the ones defined in (Chiou et al., 2012; Farhadifar et al., 2007). More precisely, an energy function dependent on the positions of the cell vertices is defined as $E=\sum_i(A_i-A_i^0)^2+\Gamma P_i$, where A_i, A_i^0 *and* P_i are respectively the area, intial area and perimeter of cell *i*, and Γ is a scalar. This accounts for the fact that cells usually maintain their volume (or area in 2D) while minimizing their circumference, thus keeping a roundish shape. The vertices are then moved down the gradient of the energy function. For the first set of lattices, random T1 transitions (or neighbor swaps, see Staple et al.(Staple et al., 2010)) are performed to break the symmetry of the lattice. Small cells (in our case if $A_i<A_i^0/4$) are removed from the lattice. For the random hexagonal lattices (Fig. S4A), the A_i^0 are multiplied by a cell specific factor drawn from a uniform distribution between 0.5 and 2 to ensure that cells have different sizes but the same number of neighbors.

Quantification and Statistical Analysis

Image analysis—All data processing was performed off-line using a commercial software package (MATLAB R2016, the MathWorks Inc.). A semi-automatic analysis code was used for cell segmentation and data extraction. N1G4-citrine and Dll1-mCherry cells were segmented separately using the yellow (515nm laser) and red (561nm laser) channels, respectively. For the two-cell assay, TEC was defined as total fluorescence in the yellow channel (green in images shown) found in the area of the Dll1-mCherry cell. Background fluorescence, calculated from pixels outside the segmented area, was subtracted from the TEC signal. Fluorescence signal from the boundary between cells as defined by the overlap of the segmentation of the two cells, was not included in the calculation of TEC. This is because we consider as TEC only N1G4-Citrine within the sender cell and not on the boundary. nTEC was calculated by dividing the TEC by total Dll1-mCherry signal in each time frame. The correlation coefficient between nTEC and contact width and the corresponding p-value was estimated using Pearson correlation analysis. The reporter analysis (Fig. S1N-P) was performed by a semi-automatic tracking protocol in which the total fluorescence in the nucleus was calculated in each frame.

Estimation of contact width in the two-cell assay—The contact area between cells was assumed to be proportional to the contact width visible within the plane that was analyzed. For the data on Fig 3, the contact width was estimated by averaging over the first 10 time points of the movie. For the data on Fig S3 showing max nTEC, the contact width

Europe PMC Funders Author Manuscripts

was estimated by averaging over measured the 10 time points prior to the time point where max nTEC was measured. For some cases, where the max nTEC is earlier that the 10^{th} time point, we used an average of the first 10 time points. We checked that the standard deviation on width measurements were relatively small. Cases in which large changes in the contact width occurred within the averaging time were not used in the analysis.

Image analysis for chick basilar papilla—Images of cingulin labeled cells (such as the one in Fig S4J) were initially segmented using ilastik program (Sommer et al., 2011). The segmentation was then refined and semi-automatically corrected using a custom made code in Matlab (the MathWorks Inc.). Cells expressing HCA were manually marked on segmented image. Distributions of cell perimeters were then extracted and analyzed. Wilcoxon rank sum test was then applied to determine the significance of the difference between the distributions of cells expressing or not expressing HCA.

Statistics—Calculation of correlations and their p-value: Statistical analysis of Figs 3, 4D and S3 was performed using Pearson correlation. Analysis in Figs 4C, 4F, S4B and S4I were performed using Wilcoxon rank sum test. The time delays and delayed correlations in Fig. S1P were calculated by finding the shift in time required to reach the maximal correlation coefficient between the two data sets. The correlation was calculated using Pearson correlation over the overlapping data points after time shifting. The number of samples is as indicated in each figure caption.

Supplementary Material

Refer to Web version on PubMed Central for supplementary material.

Acknowledgment

We would like to thank Olga Loza for help with the experiments. We would like to thank Irwin Bernstein for kindly providing Dll1-Fc for the Notch activity test. We also thank Boris Shraiman for providing MATLAB functions that helped generate random cell lattices. This work was supported by grants from the Israeli Science Foundation (grant no. 1021/11), and a European Research Council grant (grant no. 682161). G.R. and R.G. acknowledge support by the Wellcome Trust fund (grant no. 087377).

References

Akanuma T, Chen C, Sato T, Merks RM, Sato TN. Memory of cell shape biases stochastic fate decision-making despite mitotic rounding. Nat Commun. 2016; 7:11963. [PubMed: 27349214]

Andrawes MB, Xu X, Liu H, Ficarro SB, Marto JA, Aster JC, Blacklow SC. Intrinsic selectivity of Notch 1 for Delta-like 4 over Delta-like 1. J Biol Chem. 2013; 288:25477–25489. [PubMed: 23839946]

Artavanis-Tsakonas S, Muskavitch MA. Notch: the past, the present, and the future. Curr Top Dev Biol. 2010; 92:1–29. [PubMed: 20816391]

Artavanis-Tsakonas S, Rand M, Lake R. Notch Signaling: Cell Fate Control and Signal Integration in Development. Science. 1999; 284:770. [PubMed: 10221902]

Benhra N, Vignaux F, Dussert A, Schweisguth F, Le Borgne R. Neuralized promotes basal to apical transcytosis of delta in epithelial cells. Mol Biol Cell. 2010; 21:2078–2086. [PubMed: 20410139]

Bentley K, Mariggi G, Gerhardt H, Bates PA. Tipping the balance: robustness of tip cell selection, migration and fusion in angiogenesis. PLoS Comput Biol. 2009; 5:e1000549. [PubMed: 19876379]

Bentley K, Philippides A, Ravasz Regan E. Do endothelial cells dream of eclectic shape? Dev Cell. 2014; 29:146–158. [PubMed: 24780735]

Bray S. Notch signalling: a simple pathway becomes complex. Nat Rev Mol Cell Biol. 2006; 7:678–689. [PubMed: 16921404]

Chiou KK, Hufnagel L, Shraiman BI. Mechanical stress inference for two dimensional cell arrays. PLoS Comput Biol. 2012; 8:e1002512. [PubMed: 22615550]

Cohen M, Georgiou M, Stevenson NL, Miodownik M, Baum B. Dynamic filopodia transmit intermittent Delta-Notch signaling to drive pattern refinement during lateral inhibition. Dev Cell. 2010; 19:78–89. [PubMed: 20643352]

Collier JR, Monk NA, Maini PK, Lewis JH. Pattern formation by lateral inhibition with feedback: a mathematical model of delta-notch intercellular signalling. J Theor Biol. 1996; 183:429–446. [PubMed: 9015458]

Couturier L, Vodovar N, Schweisguth F. Endocytosis by Numb breaks Notch symmetry at cytokinesis. Nat Cell Biol. 2012; 14:131–139. [PubMed: 22267085]

D'Souza B, Meloty-Kapella L, Weinmaster G. Canonical and non-canonical Notch ligands. Curr Top Dev Biol. 2010; 92:73–129. [PubMed: 20816393]

Desai RA, Gao L, Raghavan S, Liu WF, Chen CS. Cell polarity triggered by cell-cell adhesion via E-cadherin. J Cell Sci. 2009; 122:905–911. [PubMed: 19258396]

Farhadifar R, Roper JC, Aigouy B, Eaton S, Julicher F. The influence of cell mechanics, cell-cell interactions, and proliferation on epithelial packing. Curr Biol. 2007; 17:2095–2104. [PubMed: 18082406]

Fleming RJ, Hori K, Sen A, Filloramo GV, Langer JM, Obar RA, Artavanis-Tsakonas S, Maharaj-Best AC. An extracellular region of Serrate is essential for ligand-induced cis-inhibition of Notch signaling. Development. 2013; 140:2039–2049. [PubMed: 23571220]

Formosa-Jordan P, Sprinzak D. Modeling Notch signaling: a practical tutorial. Methods Mol Biol. 2014; 1187:285–310. [PubMed: 25053498]

Gibson DG, Young L, Chuang RY, Venter JC, Hutchison CA 3rd, Smith HO. Enzymatic assembly of DNA molecules up to several hundred kilobases. Nat Methods. 2009; 6:343–345. [PubMed: 19363495]

Goodyear R, Richardson G. Pattern Formation in the Basilar Papilla: Evidence for Cell Rearrangement. Journal of Neuroscience. 1997; 17:6289–6301. [PubMed: 9236239]

Hamada H, Watanabe M, Lau HE, Nishida T, Hasegawa T, Parichy DM, Kondo S. Involvement of Delta/Notch signaling in zebrafish adult pigment stripe patterning. Development. 2014; 141:318–324. [PubMed: 24306107]

Hatakeyama J, Wakamatsu Y, Nagafuchi A, Kageyama R, Shigemoto R, Shimamura K. Cadherin-based adhesions in the apical endfoot are required for active Notch signaling to control neurogenesis in vertebrates. Development. 2014; 141:1671–1682. [PubMed: 24715457]

Heitzler P, Simpson P. The choice of cell fate in the epidermis of Drosophila. Cell. 1991; 64:1083–1092. [PubMed: 2004417]

Heuss SF, Ndiaye-Lobry D, Six EM, Israel A, Logeat F. The intracellular region of Notch ligands Dll1 and Dll3 regulates their trafficking and signaling activity. Proc Natl Acad Sci U S A. 2008; 105:11212–11217. [PubMed: 18676613]

Huang H, Kornberg TB. Myoblast cytonemes mediate Wg signaling from the wing imaginal disc and Delta-Notch signaling to the air sac primordium. Elife. 2015; 4:e06114. [PubMed: 25951303]

Hunter GL, Hadjivasiliou Z, Bonin H, He L, Perrimon N, Charras G, Baum B. Coordinated control of Notch/Delta signalling and cell cycle progression drives lateral inhibition-mediated tissue patterning. Development. 2016; 143:2305–2310. [PubMed: 27226324]

Jakobsson L, Franco CA, Bentley K, Collins RT, Ponsioen B, Aspalter IM, Rosewell I, Busse M, Thurston G, Medvinsky A, et al. Endothelial cells dynamically compete for the tip cell position during angiogenic sprouting. Nat Cell Biol. 2010; 12:943–953. [PubMed: 20871601]

Khait I, Orsher Y, Golan O, Binshtok U, Gordon-Bar N, Amir-Zilberstein L, Sprinzak D. Quantitative analysis of Delta-like-1 membrane dynamics elucidates the role of contact geometry on Notch signaling. Cell Reports. 2015

Kornberg TB, Roy S. Cytonemes as specialized signaling filopodia. Development. 2014; 141:729–736. [PubMed: 24496611]

Nichols JT, Miyamoto A, Olsen SL, D'Souza B, Yao C, Weinmaster G. DSL ligand endocytosis physically dissociates Notch1 heterodimers before activating proteolysis can occur. J Cell Biol. 2007; 176:445–458. [PubMed: 17296795]

Parks AL, Klueg KM, Stout JR, Muskavitch MA. Ligand endocytosis drives receptor dissociation and activation in the Notch pathway. Development. 2000; 127:1373–1385. [PubMed: 10704384]

Shaya O, Sprinzak D. From Notch signaling to fine-grained patterning: Modeling meets experiments. Curr Opin Genet Dev. 2011; 21:732–739. [PubMed: 21862316]

Sommer C, Strähle C, Köthe U, Hamprecht FA. ilastik: Interactive Learning and Segmentation Toolkit. Eighth IEEE International Symposium on Biomedical Imaging (ISBI) Proceedings. 2011:230–233.

Sprinzak D, Lakhanpal A, LeBon L, Garcia-Ojalvo J, Elowitz MB. Mutual inactivation of Notch receptors and ligands facilitates developmental patterning. PLoS Comput Biol. 2011; 7:e1002069. [PubMed: 21695234]

Sprinzak D, Lakhanpal A, Lebon L, Santat LA, Fontes ME, Anderson GA, Garcia-Ojalvo J, Elowitz MB. Cis-interactions between Notch and Delta generate mutually exclusive signalling states. Nature. 2010; 465:86–90. [PubMed: 20418862]

Staple DB, Farhadifar R, Roper JC, Aigouy B, Eaton S, Julicher F. Mechanics and remodelling of cell packings in epithelia. Eur Phys J E Soft Matter. 2010; 33:117–127. [PubMed: 21082210]

Thiery JP. Epithelial-mesenchymal transitions in development and pathologies. Curr Opin Cell Biol. 2003; 15:740–746. [PubMed: 14644200]

Europe PMC Funders Author Manuscripts

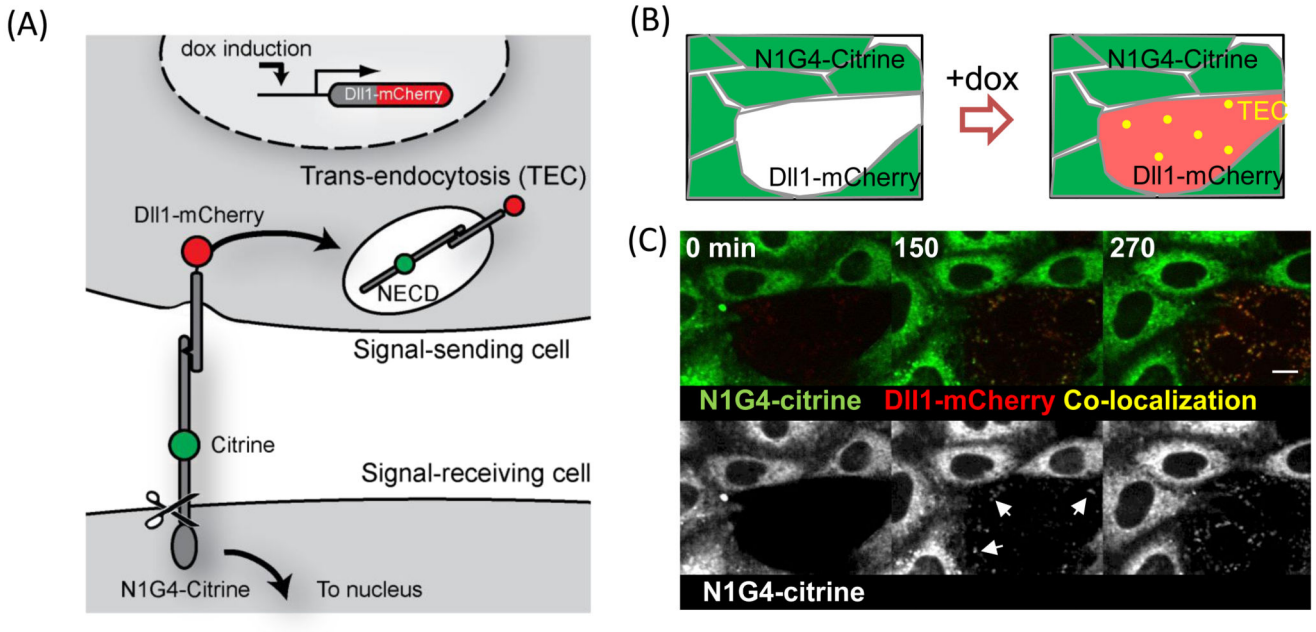

Figure 1. The live-cell Notch trans-endocytosis (TEC) assay allows dynamic tracking of N1-Dll1 interaction.

(A) A schematic of the Notch TEC assay. In this assay a signal sending cell expressing Dll1-mCherry (gray-red, top) under a doxycycline inducible promoter is co-cultured with a signal receiving cell expressing N1G4-citrine (gray-green, bottom). The N1G4-citrine has a citrine (green) inserted in the extracellular domain of N1 (NECD) and Gal4 replacing its intracellular domain. Upon Interaction between Dll1-mCherry and the N1G4-citrine the extracellular domain of N1G4-citrine trans-endocytoses into the Dll1-mCherry cell. **(B)** A schematic of a co-culture experiment. N1G4-Citrine cells (green) are co-cultured with Dll1-mCherry cells (white/red). At the beginning of the experiment Dll1-mCherry is induced by doxycycline. Upon induction of Dll1-mCherry, trans-endocytosed vesicles (yellow) appear in signal sending cells. **(C)** A filmstrip showing a co-culture experiment as described in (B). Here, Dll1-mCherry (red) cells are co-cultured with N1G4-ctirine cells (green in the top row, gray in the bottom row) (see also Movie S1). The bottom row shows only the N1G4-citrine. Dll1-mCherry cells (red) were pre-induced with 100 ng/mL of doxycycline 3 hr prior to the first frame (t = 0). TEC is observed as vesicles containing both N1G4-citrine and Dll1-mCherry within the Dll1-mCherry cells (yellow in the top row, arrows in the bottom row). Scale-bar 10μm. See also associated Figure S1.

Europe PMC Funders Author Manuscripts

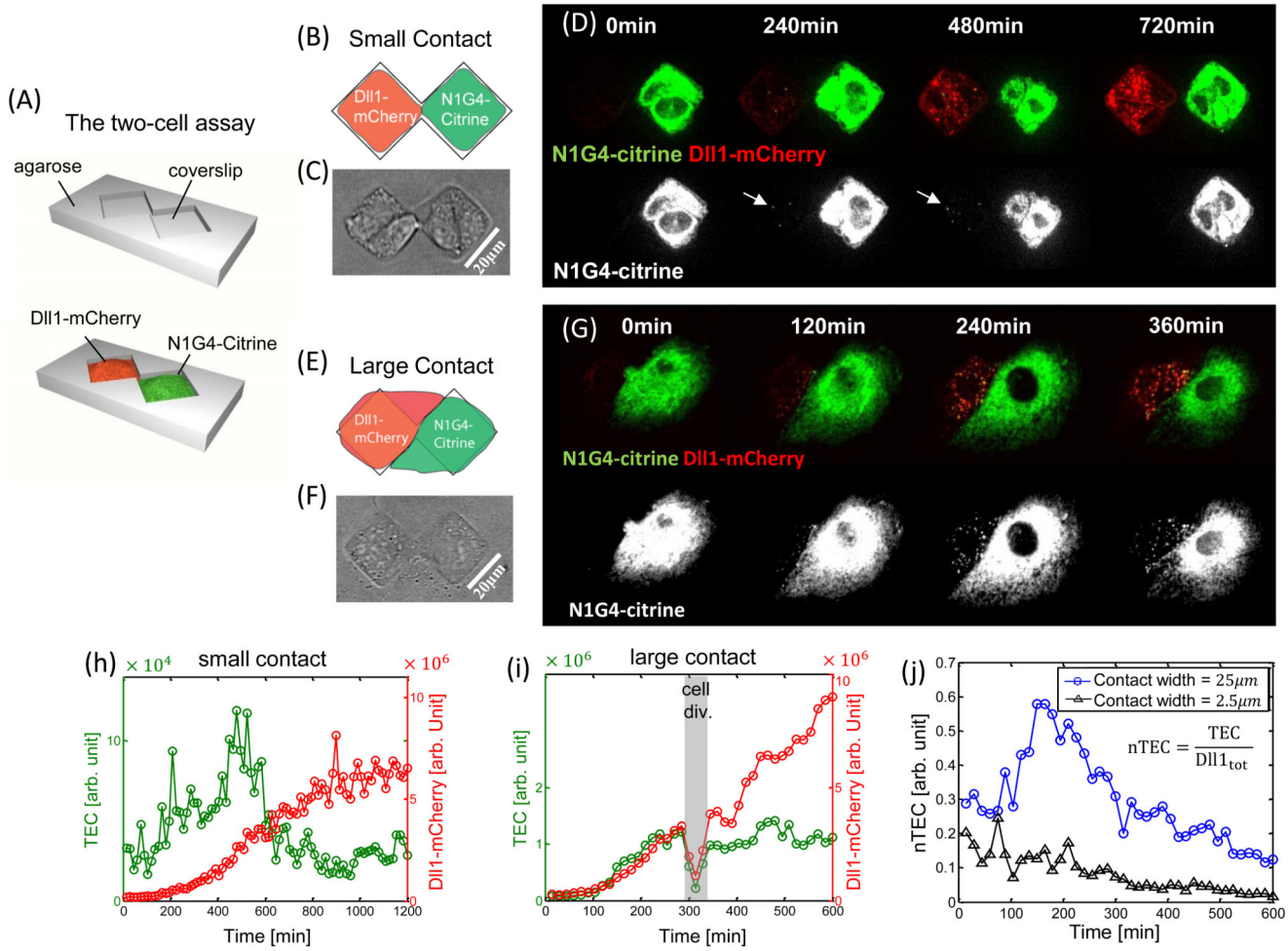

Figure 2. The two-cell TEC assay allows measuring the dependence of TEC on contact width.

(A) A schematic of the device used for the two-cell assay. **(B)** A schematic of a two-cell TEC assay in a pair of cells with small contact width (~2.5 μm). **(C)** A bright field image of the cell pair used in (D). Scale-bar as indicated **(D)** A filmstrip showing a Dll1-mCherry cell (red) and a N1G4-citrine cell (green in top row, gray in bottom row) interacting in a two-cell microwell (see movieS2 in supplementary). Bottom row shows only the N1G4-citrine fluorescence. Dll1-mCherry was pre-induced with 100 ng/ml doxycycline one hour prior to the first frame of the movie (t=0). Arrows indicate TEC events. **(E)** A schematic of a two-cell TEC assay on a pair of cells with large contact width. In this experiment, cells broke out of the microwells and formed a large contact (~25 μm length). **(F)** A bright field image of the cell pair used in (G). Scale-bar as indicated. **(G)** A filmstrip showing TEC in a pair of cells with a large contact width (see movie S3 in supplementary). Experimental procedure and labeling is the same as shown in (D). **(H-I)** Quantitative analysis of the filmstrips in (D) and (G), respectively. The levels of TEC (green, left axis) and Dll1-mCherry fluorescence (red, right axis) are plotted as a function of time. Grayed area in (F) indicate cell division period, where cells are partially out of the image plane. **(J)** Comparison of the normalized TEC (nTEC) between small and large contact widths (i.e. between (H, black) and (I, blue)).

nTEC is defined as the level of TEC divided by total Dll1-mCherry level. See also associated Fig. S2.

Europe PMC Funders Author Manuscripts

Europe PMC Funders Author Manuscripts

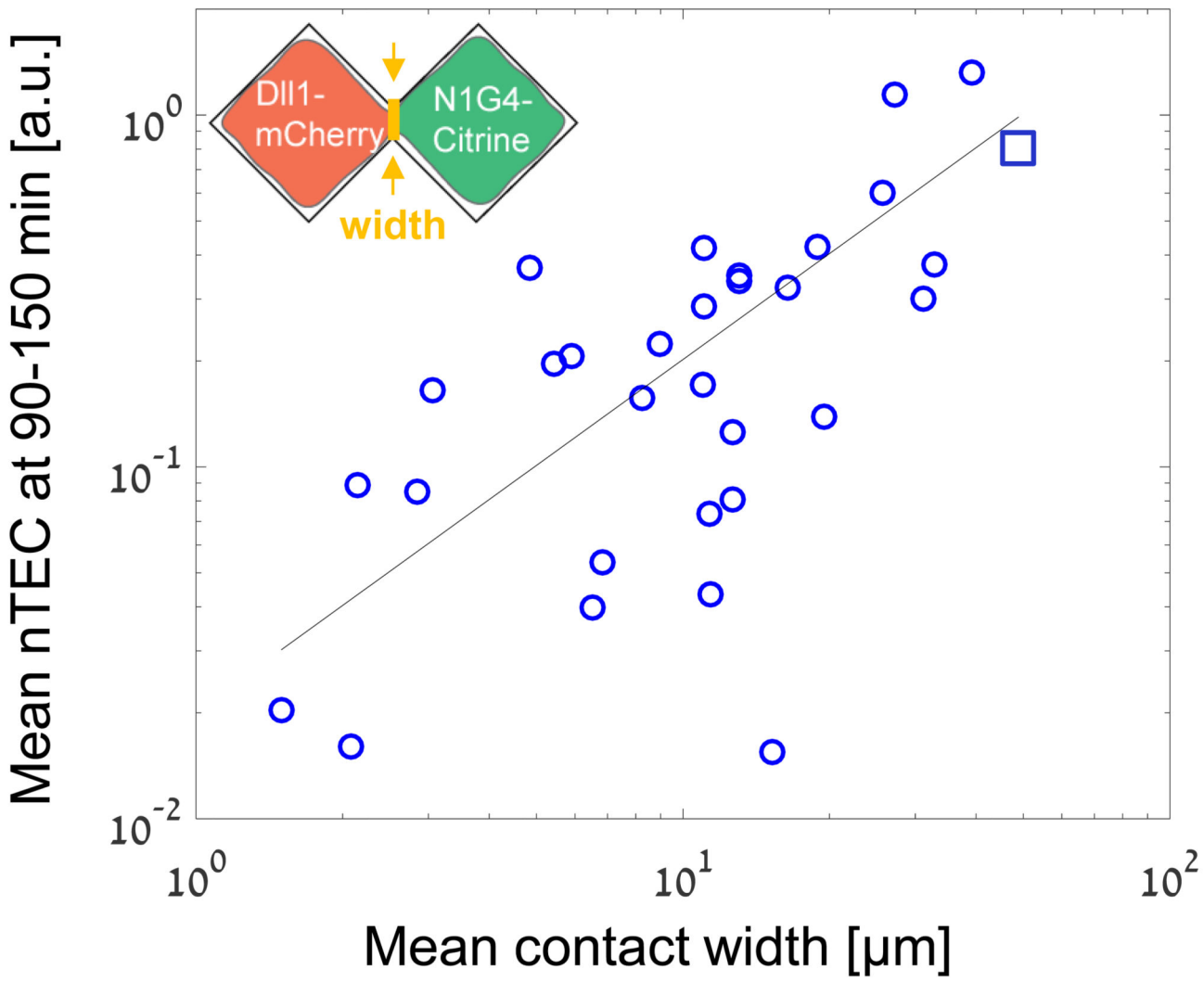

Figure 3. nTEC is correlated with contact width.

A plot showing the mean nTEC level between 90-150 min after the movie started, as a function of the mean contact width between 0-150 min (in both cases the mean is taken over time). Data shown is from 30 two-cell assay experiments (as in Fig. 2D,G, circles) and one data point from a free co-culture experiment (square). The solid line is a linear fit to the data points. This data shows that nTEC levels correlate with the width of the contact between the cells (n=31, ρ=0.83, p-value<10^{-8} calculated using Pearson correlation). See also associated Fig. S3.

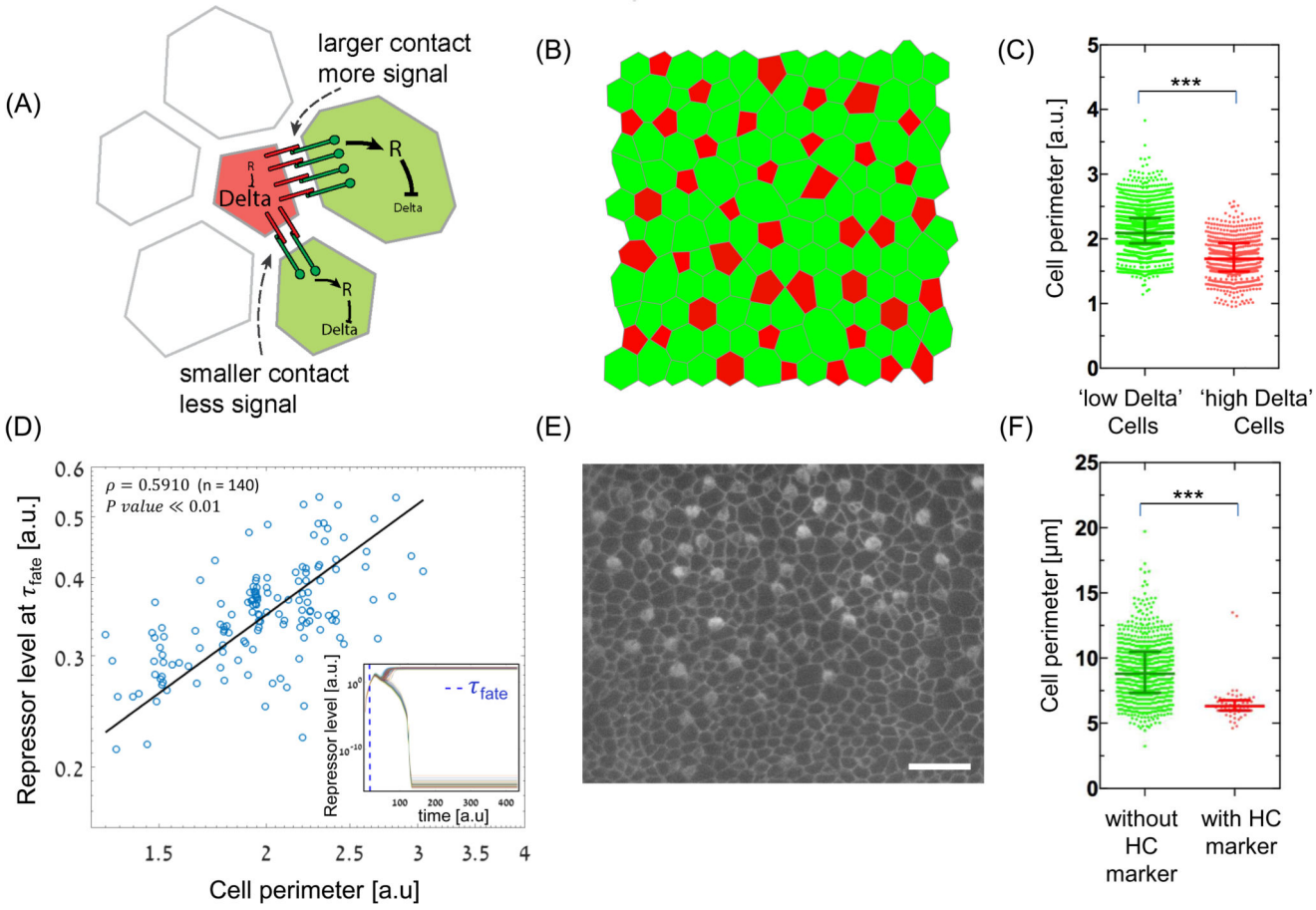

Figure 4. Dependence of Notch signaling on contact area can bias lateral inhibition patterning.

(A) A schematic of a model for lateral inhibition that takes into account dependence of signaling on contact area. The model assumes that Notch signaling in each cell depends on the number of Notch-Delta pairs formed (red and green, respectively). Notch signaling in each cell activates a repressor (R) that inhibits Delta production. Finally, Delta is distributed evenly on cell boundaries. **(B)** A simulation of the lateral inhibition model shown in (A) on a disordered cell lattice. Cells that express high levels of Delta are red and cells that express low level of Delta are green. The simulation was performed as described in the STAR methods (Eqs. 15-17). Parameters used: $\beta_N = 3.9$, $\beta_D = 3.9$, $\beta_R = 194.1$, m = 3, l = 3, $k_t^{-1} = 0.2$ **(C)** A histogram showing the distribution of cell perimeters for high-Delta cells (red, n=827) and low Delta cells (green, n=1974) collected from simulations on 20 random lattices. **(D)** Analysis of the dynamics of the simulation in (B) showing a correlation between repressor level (R in (A)) and cell perimeter, at the fate determination point, τ_{fate} (n=140, ρ=0.59, p-value<10^{-13} calculated using Pearson correlation). The solid line is a linear fit to the data points. Inset: a plot of repressor levels for each cell as a function of time. The fate determination point, τ_{fate} (dashed line), is defined as the latest time where there is no significant difference in the Delta levels of the prospective high and low Delta cells. **(E)** An image from the distal region of the chick basilar papilla taken at E6 (from (Goodyear and Richardson, 1997)). Samples were stained using both anti-cingulin (membrane/tight junction

Europe PMC Funders Author Manuscripts

marker) and anti-HCA (Hair cell marker). Scale-bar 10μm. **(F)** A histogram of cell perimeters in (E) showing that cell with hair cell (HC) marker (red, n=62) have smaller apical perimeters on average than cells without HC marker (green, n=732). See Fig. S4J-L and methods for description of analysis. In (C) and (F) the middle bar and error bars denote the median and interquartile range, respectively. Three stars denote p-value<0.001 determined by Wilcoxon rank sum test. See also associated Fig. S4.

Europe PMC Funders Author Manuscripts

Europe PMC Funders Author Manuscripts

Key Resources Table

REAGENT or RESOURCE	SOURCE	IDENTIFIER
Antibodies		
anti-mouse-Notch1 (1:100)	R&D Systems	AF5267; RRID: AB_1655874
Alexa Fluor 488-conjugated AffiniPure Rabbit-anti-Sheep (1:200)	Jackson ImmunoResearch	313-545-003; RRID: AB_2340013
anti-cingulin	Goodyear and Richardson, 1997	N/A
anti-HCA	Goodyear and Richardson, 1997	N/A
Chemicals, Peptides, and Recombinant Proteins		
Delta-like 1 fused to immunoglobin-G (Dll1-Fc)	kind gift from Irwin Bernstein	N/A
Doxycycline	Sigma Aldrich	D9891-1G
Paraformaldehyde	Merck	30525-89-4
Triton X100	Sigma Aldrich	9002-93-1
Blasticidine	A.G. Scientific	B-1247-SOL
Geneticin	Life Technologies	108321-42-2
Zeocin	Invivogen	Ant-zn
Hygromicine	A.G. Scientific	H-1012-PBS
PDMS	Dow Corning	3097358-1004
Agarose	Lonza	50004
Bovine Fibronectin	Biological Industries, Israel	03-090-1-01
αMEM	Biological Industries, Israel	01-042-1A
Fetal bovine serum, 10%	Biological Industries, Israel	04-007-1A
Low fluorescence imaging media (αMEM without Phenol red, ribonucleosides, deoxyribonucleosides, folic acid, biotin and vitamin B12)	Biological Industries, Israel	06-1042-18-1A
Magnesium carbonate hydroxide pentahydrate	Sigma Aldrich	467480
Tricine	Sigma Aldrich	93356
EDTA	Biological Industries, Israel	V4233
MgSO4	Merck	106067
ATP	Sigma Aldrich	A2383
DTT	Sigma Aldrich	D9779-5G
Coenzyme A	Sigma Aldrich	C3144-10mg

Europe PMC Funders Author Manuscripts

REAGENT or RESOURCE	SOURCE	IDENTIFIER
D-Luciferine	Regis Technologies	1-360222-200
di-Potassium hydrogen phosphate trihydrate	Merck	1.05099.1000
Potassium dihydrogen phosphate	Merck	1.04873.1000
Passive lysis buffer	Promega	E194A
Critical Commercial Assays		
TransIT-LT1 transfection kit	Mirus	MIR-2305
Platinum pfx PCR kit	Life Technologies	11708-013
Experimental Models: Cell Lines		
Hamster: CHO-Dll1-mCherry	ATCC & Life Technologies	CCL-61, CHO-TR
Canine: MDCK-Dll1-mCherry	ATCC	CRL-2936
CHO-N1G4-citrine	This paper	N/A
CHO-N1G4-citrine+UAS-H2B-mCherry	This paper	N/A
CHO-N1G4esn	Sprinzak et al., 2010	N/A
Experimental Models: Organisms/Strains		
Chick Basilar Papilla (E6 and E8)	Goodyear and Richardson, 1997	N/A
Oligonucleotides		
Primers for citrine insert 5-ACTACAGCTTCGGGGGTGGGGGTTCAGGTATGGTGAGCAAGGGCGAGGAG-3’ 5’-GGGGGATGTCGCGCCCGGCCCCAGATCCCTTGTACAGCTCGTCCATGCC-3’	This paper	N/A
Primers for 3 overlapping fragments for pcDNA3-hNECD-Gal4esn 5’- CGAGCTGTACAAGGGATCTGGGGCCGGGCGCGACATCCCCC-3’ 5’- CCCTTGCTCACCATACCTGAACCCCCACCCCCGAAGCTGTAGT-3’ 5’- GACCATGATTACGCCAAGCTCTAG-3’ 5’- CATGTCTGTATACCGTCGACCTCTAG-3’ 5- CAGTTGGGGCCAGTGTGGGTG-3’ 5- CTACCGCTGCGTCTGCCGCGC-3’	This paper	N/A
Recombinant DNA		
pcDNA5TR-rDll1-mCherry	Sprinzak et al., 2010	N/A
pcDNA3-hN1	Sprinzak et al., 2010	N/A
pcDNA3-N1G4	N1G4esn from Sprinzak et al., 2010	N/A
pcDNA3-N1G4-citrine	This paper	N/A
pEV-UAS-H2B-mCherry	This paper	N/A
Gal4-firefly luciferase reporter	Andrawes et al., 2013	N/A

Europe PMC Funders Author Manuscripts

REAGENT or RESOURCE	SOURCE	IDENTIFIER
pRL-SV40	Promega	E2231
Software and Algorithms		
MATLAB	MathWorks	R2016
Code for lateral inhibition simulation	https://github.com/Udi-Binshtok/Dimensionless-equations-simulator_-February-2017.git	N/A
Other		
UV/Ozone cleaning device	UVOCS, USA	N/A